JOURNAL OF GEOPHYSICAL RESEARCH, VOL. 103, NO. D14, PAGES 17,033–17,039, JULY 27, 1998

Synthetic spectra for terrestrial ultraviolet from discrete measurements

Qilong Min and Lee C. Harrison

Atmospheric Sciences Research Center, State University of New York at Albany

Abstract. We describe a rapid inversion algorithm for constructing synthetic terrestrial spectra from measurements made by instruments with multiple narrowband detectors. We show tests of algorithm performance over large dynamic ranges of ozone amount, solar zenith angle, surface albedo, and optical depths of aerosol and clouds. These tests demonstrate that the accuracy of synthetic spectra for total, diffuse, and direct irradiances will be limited by instrument accuracy in almost all cases. Consequently, we show uncertainty analyses for the effects of measurement and calibration errors (including filter wavelength shifts), and the impact of filter wavelength selection on the inverted spectra.

1. Introduction

In view of the harmful biological effects expected from increased UV radiation at the Earth surface and changes in important photochemical reaction rates in the troposphere due to ozone depletion, it is vitally important to investigate the increases in biologically damaging UV irradiance at the surface [*WMO*, 1994; *United Nations Environment Program (UNEP)*, 1991].

Terrestrial ultraviolet radiometers with multiple relatively narrow passbands defined by interference filters [*Correll et al.*, 1992; *Bigelow et al.*, 1998] are now widely distributed for the purpose of long-term measurements. These instruments provide much greater spectral information than a UV-B pyranometer, without the cost and operational complexity of a UV spectrometer. However, to use data obtained from a multiple-discrete passband instrument, we need a technique to accurately estimate the continuous spectral distribution [*Michalsky and Kleckner*, 1984] and to predict the irradiance integral for arbitrary action spectra from the data. The problem of correct generation of synthetic spectra is also closely related to the retrieval of the relevant physical properties of the atmosphere which control the radiative transmission at these wavelengths [*Dahlback*, 1996; *Booth*, 1997]. For the UV these are the ozone column (and secondarily several other less important trace gases), as well as aerosol and cloud optical depths versus wavelength.

Here we present a technique for constructing synthetic terrestrial spectra to arbitrary resolution, given data from a well-calibrated and characterized multifilter radiometer. This method does not depend on an explicit forward calculation of radiative tranfer through the atmosphere; thus the algorithm is fast and avoids the necessity for detailed descriptions of the atmospheric state. Nonetheless we show that this algorithm produces results with accuracies dominated by instrument calibration over large dynamic ranges for various atmospheric conditions. We also discuss the impact of filter drifts and filter selection.

Paper number 98JD01452.
0148-0227/98/98JD-01452$09.00

2. Construction Method

2.1. General Approach

The examples shown here specifically describe data available from the UV-MFRSR instruments deployed in the (USDA) which are the ultraviolet version of the multifilter rotation shadowband radiometer (MFRSR) [*Harrison et al.*, 1994]. This instrument measures spectral direct, diffuse, and total horizonal irradiances at 300, 305, 312, 317, 325, 333, and 367 nm with passbands $\approx$ 2.5 nm (FWHM).

The measured irradiance from the UV-MFRSR can be written as

$$b_i = \int_0^\infty F_i(\lambda)\rho(\lambda)d\lambda \qquad i = 1, 2, \cdots, m \qquad (1)$$

where F is the filter (or responsivity) function of instrument at corresponding wavelength, and ρ is the spectrum received at the surface. The inversion of the surface spectrum from a multifilter instrument appears as a first-order Fredholm integral equation [*Chahine*, 1977]. To solve this problem we must use prior physical information about radiative transfer and the physical system as constraints. To do so, we write the estimated spectrum ρ' as

$$\rho'(\lambda, \mathbf{X}) = S(\lambda)T(\lambda, \mathbf{X}) \qquad (2)$$

where S and T are the solar spectrum at the top of the atmosphere (TOA) and the transmittance of the atmosphere, respectively. $\mathbf{X}$ represents the parameters in a function we choose to define the transmittance.

The practicality of this inversion hinges upon the fact that most of the structure seen in a terrestrial spectrum is either that of the extraterrestrial spectrum or due to ozone absorption, both of which have stable spectra. The effects of scattering and absorption by aerosols, clouds, and the Earth's surface produce much smoother variation in transmittance with respect to wavelength.

The difference between the synthetic spectrum and the true spectrum is

$$\epsilon(\lambda) = \rho(\lambda) - \rho'(\lambda, \mathbf{X}) \tag{3}$$

or multiplying both sides with filter functions, then we have

$$e_i = b_i - \int_0^\infty F_i(\lambda) S(\lambda) T(\lambda, \mathbf{X}) d\lambda \tag{4}$$

where

$$e_i = \int_0^\infty F_i(\lambda) \epsilon(\lambda) d\lambda$$

These, $\mathbf{X}$, coefficients, therefore can be determined in the least squares sense to minimize

$$\frac{1}{m} \sum_{i=1}^{m} e_i^2 \tag{5}$$

Having solved for the unknown coefficients, $\mathbf{X}$, we can then easily construct the synthetic spectrum from equation (2).

2.2. Transmittance Function

Here we explain our transmittance function as based on approximations to the fundamental problem; but equally, our transmittance function can be seen as an arbitrary choice, justified only retrospectively by its ability to handle the range of test cases shown.

In the general transmittance problem for the diffuse irradiance there will be a distribution of photon pathlengths through the atmosphere to the terrestrial radiometer. The transmittance with the gaseous absorption in multiple scattering-processes can be written as

$$T(\lambda) = T_c(\lambda) \int_0^\infty p(u) e^{-K^{O3}(\lambda) u} du$$

For our purpose we assume

$$T(\lambda) = T_c(\lambda) e^{-K^{O3}(\lambda) < u >} \tag{6}$$

where $T_c(\lambda)$ is the transmittance without the gaseous absorption; $p(u)$ is the photon pathlength distribution; and $< u >$ is the average photon pathlength in the atmosphere. $K^{O3}(\lambda)$ is the ozone absorption coefficients as a function of wavelength.

The wavelength dependency of optical depths due to Rayleigh scattering, aerosol and cloud extinction are of the form

$$\tau(\lambda) = \beta \lambda^{-\alpha}$$

Rayleigh scatterers are characterized by $\alpha \approx 4$, whereas $\alpha \approx 0$ for large scatterers like cloud particles [*Stephens*, 1994]. Therefore we assume the transmittance without gaseous absorption to be

$$T_c(\lambda) = \exp[-\sum_{i=0}^{4} x_i (\frac{1}{\lambda})^i] \tag{7}$$

The photon pathlength for the direct-beam irradiance is directly determined by the solar zenith angle. However, for the diffuse irradiance it varies modestly (over this relatively narrow wavelength range) with wavelength according to the change of multiple scattering with wavelength, and we assume

$$< u >= a + b(\frac{1}{\lambda}) \tag{8}$$

then we have

$$T(\lambda, \mathbf{X}) = \exp[-\sum_{i=0}^{4} x_i (\frac{1}{\lambda})^i - K^{O3}(\lambda)(x_5 + x_6(\frac{1}{\lambda}))] \tag{9}$$

Therefore the basis function for total, diffuse, and direct irradiances at the surface is

$$\rho'(\lambda, \underline{X}) = S(\lambda) \exp[-\sum_{i=0}^{4} x_i (\frac{1}{\lambda})^i - K^{O3}(\lambda)(x_5 + x_6(\frac{1}{\lambda}))] \tag{10}$$

Equation (10) provides an analytical formulation of the basis function for the problem of inverting the surface spectrum from multiple-filter data, which is suitable for direct, diffuse, and total irradiances under a wide range of atmospheric conditions. Substituting equation (10) into equation (4), we can determine the unknown parameters based on a nonlinear least squares method.

We use two radiative transfer models to compute "realistic" surface UV spectra for a wide range of conditions for direct, diffuse, and total irradiances. We developed one of these, a model based on the discrete ordinate method [*Stamnes et al.*, 1988], including the (SUSIM) extraterrestrial solar spectrum at 0.05 nm interval with 0.15 nm resolution [*VanHoosier et al.*, 1988] and the Bass and Paur ozone cross-section data [*Bass and Paur*, 1981]. However, the wavelength range of this model is limited by the SUSIM solar spectrum to wavelengths shorter than 403 nm. Consequently we also modified MODTRAN3.5 [*Berk et al.*, 1989] to be able to output irradiances at the surface as our forward model for the entire solar spectrum.

For the spectral synthesis computations we again use the Bass and Paur ozone cross sections and the Air Force Geophysics Laboratory (AFGL) midlatitude winter model [*Anderson et al.*, 1986] to compute the ozone absorption coefficients as a function of wavelength for one atmospheric path. We use either the SUSIM extraterrestrial solar spectrum or the solar spectrum from MODTRAN3.5 as noted.

For the artificial case of filter passbands that are δ functions, the problem can be transformed to a linear retrieval in ln(transmittance); effectively, this becomes

a problem of superposition of optical depths. In the case of the UV-MFRSR and other cited filter radiometers the filter functions are sufficiently narrow that the set of equation (4) is only weakly nonlinear; a first-guess solution based on the δ function approximation for the filter-center wavelengths serves as an efficient seed for iteration and demonstrates uniqueness of solution for adequately narrow filters. Subsequent iteration is done using the Levenberg-Marquardt method [*Press et al.*, 1989] to solve the full nonlinear problem.

3. Test Cases

From a spectrum computed by the radiative transfer models we can then simulate the instrument output for all channels by computing product integrals of the spectrum with appropriate filter functions. The following examples show Gaussian filter functions with a width of 2.5 nm FWHM, as well as the measured filter functions of one UV-MFRSR instrument. As shown later, noise and other errors can be added to the simulated measurement. The performance of the algorithm is then tested by using the simulated measurements and filter functions as inputs to the inversion and by comparing the resulting reconstructed spectra with the original modeled spectra for a wide range of conditions.

Under clear-sky conditions the total ozone amount and the solar zenith angle (SZA) are the most important factors on the surface UV irradiances, while aerosol and surface albedo play relatively minor roles. Figure 1 shows a case computed by DISORT with an ozone column of 350 (DU) and aerosol loading to yield a visibility of 45 km. The solar zenith angle is 36°, and surface albedos are 0.2 for all wavelengths. The vertical lines in the figure show the positions of the filters; the dots indicate the simulated instrument outputs for total, diffuse, and direct irradiances. Forward spectra and synthetic spectra are overlaid for direct, diffuse, and total components. The differences are extremely small, less than 0.5% for most wavelengths. Even for the wavelengths outside the filter range the synthetic spectra are better than 5% at 295 nm and 2.5% at 400 nm.

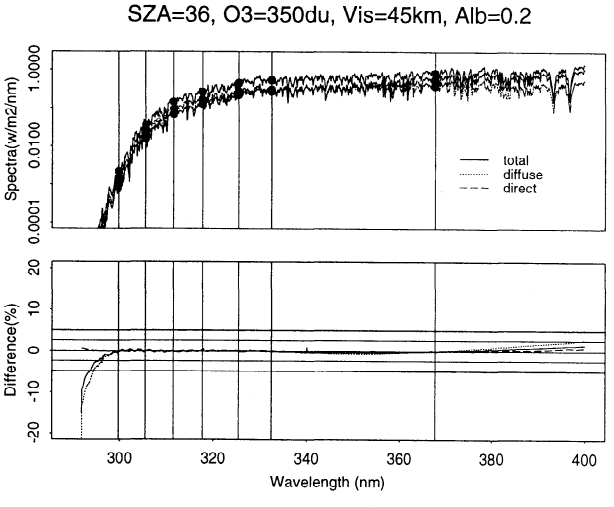

Figure 1. Comparison of forward spectra and synthetic spectra for direct, diffuse, and total irradiances for the total ozone amount of 350 DU (O3), the solar zenith angle of 36°(SZA), the visibility of 45 km (Vis), and the surface albedo of 0.2 (Alb). The vertical lines are the positions of filters, and the dots indicate the simulated instrument outputs for total, diffuse, and direct irradiances, respectively.

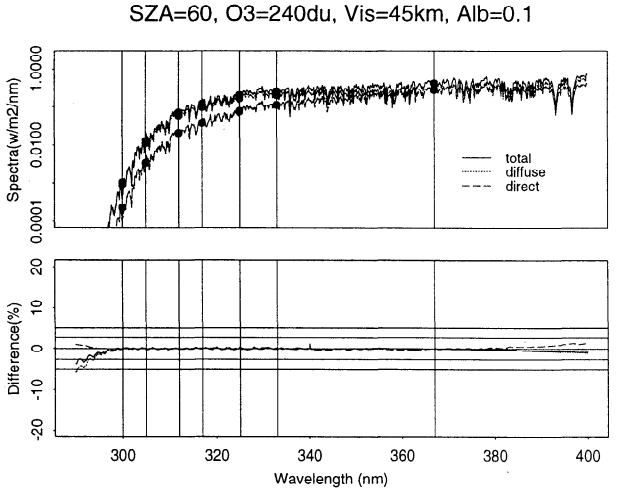

Figure 2. Same as Figure 1 but for an ozone column of 240 DU, and the key parameters are listed in the figure.

The direct-beam path length distribution is a known δ function depending on solar zenith angle. The transmittance function defined above is an exact expression for the direct irradiance given that we set the coefficient of b in equation (8) to zero. Consequently, the ozone column and aerosol optical depths inferred from direct irradiance measurements under clear-sky conditions are the best least-squares retrieval using the information from all passbands. Here the inferred total ozone and aerosol optical depths agree with the model inputs to better than 1%.

Figure 2 shows the similar case as Figure 1 but for a very low ozone amount of 240 (DU) with a solar zenith angle of 60°and a surface albedo of 0.1. Again, the differences between forward spectra and synthetic spectra are very small, indistinguishable in the top panel of Figure 2. At 290 nm the differences are less than 2.5%, 4%, and 6% for direct, total, and diffuse components.

Tests of cloudy cases are the most challenging for our algorithm. Multiple scattering in clouds enhances and greatly broadens the wavelength-dependent photon path length. These effects are most dramatic for a thick cloud layer and a high surface albedo. Figure 3 shows the case with the cloud optical depth of $\approx$ 31.5 and a surface albedo of 0.9: a value seen only for fresh snow. The solar zenith angle is 66°, and the background aerosol is set to give a visibility of 65 km. Obviously, the direct irradiances of UV are fully blocked by the cloud layer, and the diffuse irradiances are very low. Nonetheless our synthetic spectrum varies from the modeled irradiance by less than 2.5% in the spectral

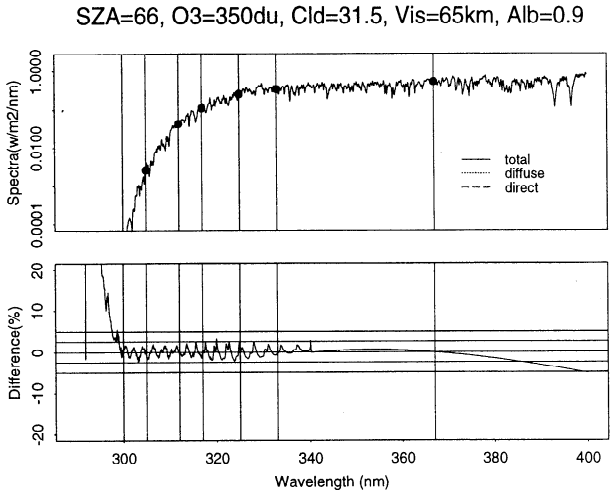

Figure 3. Same as Figure 1 but for a cloud case with the cloud optical depth of 31.5.

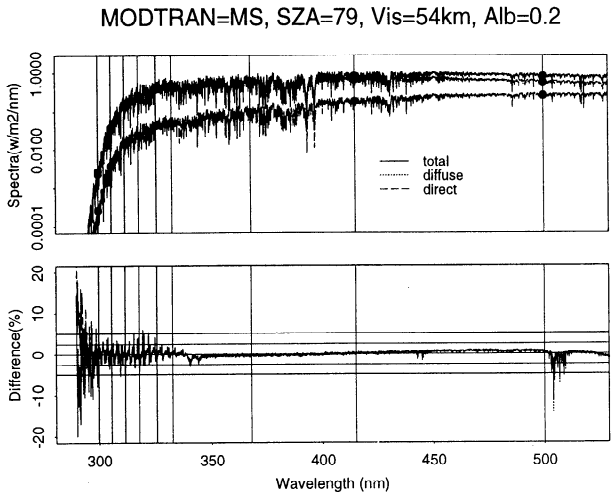

Figure 5. Same as Figure 1 but the forward spectra calculated by MODTRAN3.5 for the midlatitude summer model with the solar zenith angle of 79°.

region spanned by the measurements and is relatively good outside that region. The differences, shown in the bottom panel of Figure 3, particularly in the ozone absorption region, may be associated with a small mismatch of the mean photon path length varying with wavelength.

Many UV-MFRSRs are deployed side by side with a MFRSR; such is the case for the USDA network. Additional filter passbands from the MFRSR may assist the inversion in two ways: (1) increasing the number of inputs, increases the degree to which the solution is overdetermined; (2) a larger wavelength range should provide a more strict constraint on the basis functions for the wavelength dependency of optical properties of aerosol and cloud, resulting in a more accurate spectrum at both wavelength ends. To test the cases with additional MFRSR filters, we utilized the modified MODTRAN3.5 to compute the forward spectra.

In the following comparisons, we added two additional filters from the MFRSR at 415 and 500 nm with 10 nm FWHM passbands.

Figure 4 shows the case for the solar zenith angle at 19° under clear-sky conditions with the standard midlatitude winter atmospheric model. The aerosol optical depth was assumed to be large (visibility of 24 km), and a high surface albedo of 0.6 was assumed. In the inversion algorithm, we used the Bass and Paur ozone absorption cross sections and linearly interpolated them to the grids of the spectrum calculated by MODTRAN3.5, instead of the consistent data set of ozone absorption coefficients from MODTRAN3.5, to illustrate the uncertainty associated with ozone absorption coefficients. We used the solar spectrum at the TOA from MODTRAN3.5 in our transmittance function for the synthetic spectrum. Again, the discrepancies for total, diffuse, and direct irradiances are too small to be distin-

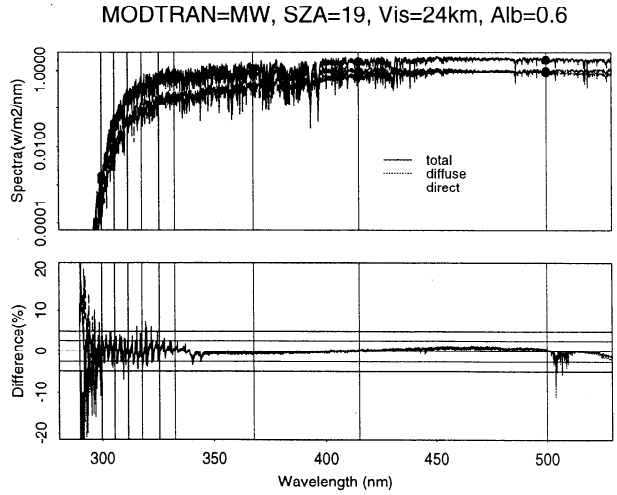

Figure 4. Same as Figure 1 but the forward spectra calculated by MODTRAN3.5 for midlatitude winter model with visibility of 24 km.

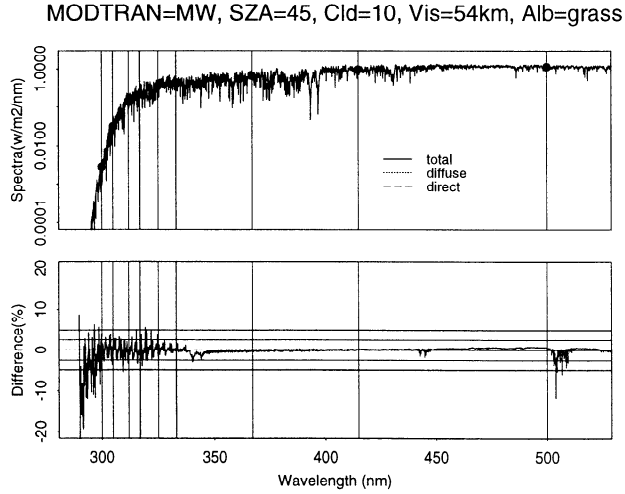

Figure 6. Same as Figure 1 but the forward spectra calculated by MODTRAN3.5 for midlatitude winter model with the cloud optical depth of 10.

guished in the top panel of Figure 4. The differences between the modeled and synthetic spectra outside the ozone absorption region are less than 1%, except for the weak H_2O absorption features near 510 nm which are not included (and could not be retrieved without a measurement in a H_2O domain) in the transmittance function for the synthesis. The small noise below 340 nm is due to inconsistency of ozone absorption coefficients used in the transmittance compared to the forward model, as discussed previously.

Figure 5 shows a case with a very high solar zenith angle of 79° and visibility of 45 km. We used the mid-latitude summer atmospheric model and assumed the surface albedo of 0.2. Again agreement is good for this extreme solar zenith angle.

Finally, we tested a case with a thick cloud layer and a surface albedo varying with wavelength. Unlike our cases with only the seven UV-MFRSR passbands, the two additional passbands from the MFRSR significantly improve the retrieval over the entire spectral range, as shown in Figure 6. The discrepancy between the synthetic spectrum and the forward spectrum is comparable to the clear-sky test cases, because of better constraint of the wavelength dependence of cloud optical properties.

4. Uncertainty Analysis

These tests over large ranges of ozone amount, solar zenith angle, surface albedo, and optical depths of aerosol and clouds demonstrate that our inversion algorithm produces accurate synthetic spectra for total, diffuse, and direct irradiances, given low measurement noise and perfect understanding of the filter functions.

However, field instruments depending on interference filters not uncommonly suffer filter drifts in both wavelength and transmittance during prolonged field operation. Further, the original calibrations for filter passband and irradiance sensitivity are difficult and may err. Hence the effects of instrument uncertainties on the accuracy of any synthetic spectrum derived therefrom are perhaps the most important question for practical application of the method.

All the following uncertainty tests are done by perturbing the simulated measurements of the case shown in Figure 1. We first studied the potential effects of instrument noise on the synthetic spectrum by adding a random magnitude error to each channel's simulated measurement from 1% to 4%. The differences are shown in Figure 7a, which illustrates that for the errors up to

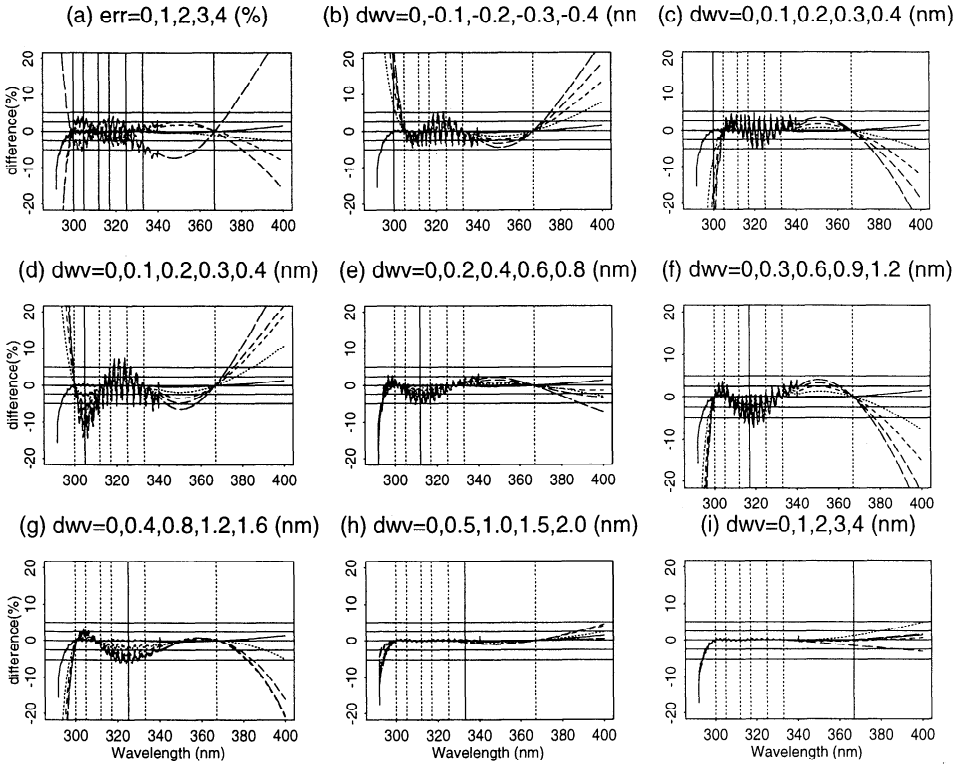

Figure 7. Differences for cases in which a random error up to 4% is added to all channels and for the cases in which the wavelength of particular filter (solid vertical line) is shifted to shorter wavelength (negative in (dwv)) or to the longer wavelength (positive in (dwv)); dwv represents the value of the wavelength shift. In each plot, the solid line represents the case without changes; the longer length of the dashed line represents the larger changes of the uncertainty of the case.

3% the synthetic spectrum is within 4% for wavelengths less than 380 nm with respect to the forward spectrum.

Potential wavelength shift of filter passbands is serious concern, particularly for the channels at shorter wavelengths where the irradiances decrease exponentially due to the ozone absorption. Figures 7b-7i show the differences due to the effects of wavelength shift on the synthetic spectrum: the vertical dotted line represents the filter without wavelength shift and the vertical solid line represents the filter with wavelength shift. As shown in Figures 7b and 7c, we shifted the wavelength of the filter at 300 nm to shorter or longer wavelength by 0.1 nm, resulting in an error of $\approx$ 6% at 300 nm.

The effect of unknown wavelength shifts of individual filters depends on the nominal wavelength of the filter in question. For nominal wavelengths greater than $\approx$ 307 nm a wavelength shift of up to 0.4 nm (at the upper end of passband shifts we have seen among interference filters in service that have not obviously failed) causes the synthetic spectrum between 305 nm and last filter (367 nm) to change by less than 5%. The wavelength shift on the longer wavelength filters has relatively small effects on the synthetic spectrum due to relatively small ozone absorption, as shown in Figures 7e-7i, particularly for filters at 330 and 367 nm.

In contrast, such a shift for filters at wavelengths less than 304 nm will substantially increase the error in the retrieved spectrum, e.g., 20% at 300 nm. A wavelength shift of 0.4 nm for the UV-MFRSR filter at 305 nm will result in 13% errors around 305 nm and up to 6% errors for some other wavelengths, as shown in Figure 7d.

The effects of filter drifts on the synthetic spectrum, particularly for the shorter wavelength filters, immediately raise the question of disregarding the data from a known erring passband. We used our algorithm with six or even five filters to construct the synthetic spectra: Figures 8a-8f show the results of differing numbers of filters and combinations.

Omitting the passband at 300 nm is of particular interest, as this measurement is the most challenging physically and the one for which the spectral synthesis shows the greatest sensitivity to passband error. As shown in Figure 8b, the spectrum retrieved without using a measurement at 300 nm is only slightly worse at wavelengths shorter than 300 nm and relatively better for the longer-wavelength end. This spectrum is much better than that retrieved using all the filters but where the first filter exhibits an unknown 0.1 nm wavelength shift.

Without the second filter the differences are barely noticeable around its central wavelength, as shown in Figure 8c. Even though we used only five filters from the third filter and above, the errors for the spectra at 300 nm are about 6% for all components, as shown in Figure 8d. It is also better than using all channels with a 0.1 nm wavelength shift in the first filter, as shown in Figures 7b and 7c. The synthetic spectrum based on other combinations of five filters show even better results than the previous case, as displayed in Figures 8e and 8f. Overall, it illustrates that we should use the channels that have accurate filter functions and calibrations rather than simply using all channels for the

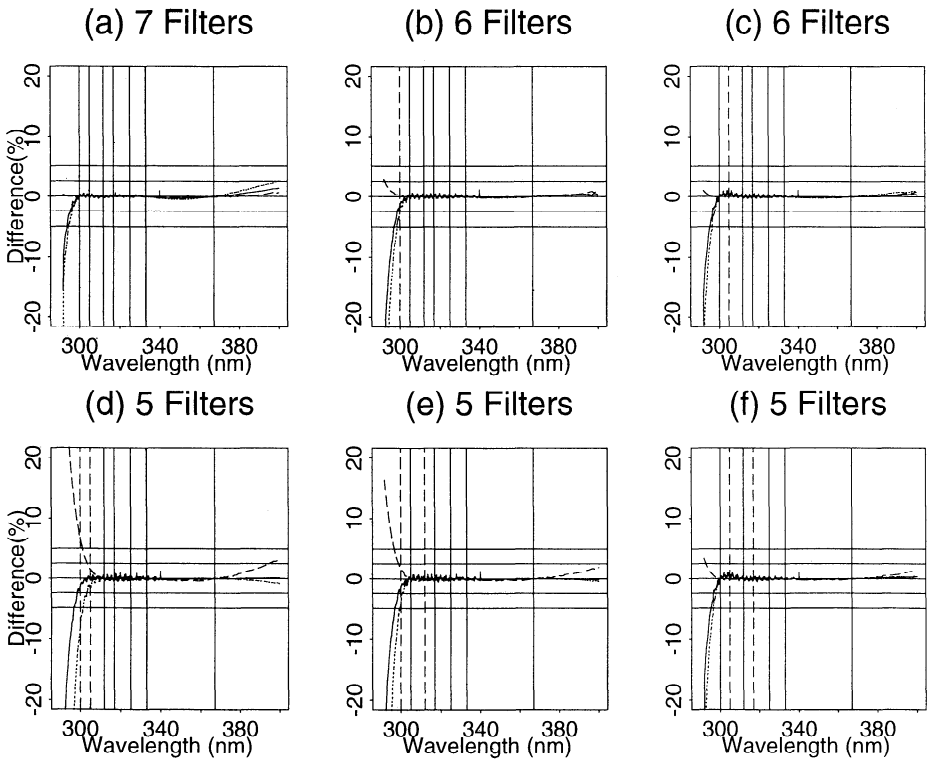

Figure 8. Illustrating the differences between the synthetic spectra and forward spectra by using five, six, and seven filters and different combinations of filters.

synthetic spectrum. This process also provides a way to check the filter calibrations by omitting individual filters in the inversion input. If a substantial change is seen in the retrieved synthetic spectrum, then the accuracy of calibration of that channel is suspect.

5. Discussion and Conclusions

We have developed an algorithm for constructing synthetic spectra from a multifilter narrowband radiometer. Tests of this algorithm over wide ranges of ozone amount, solar zenith angle, surface albedo, and optical depths of aerosol and clouds demonstrate that our inversion algorithm produces synthetic spectra for total, diffuse, and direct irradiances with errors no worse than $\approx 2\%$ at any wavelength > 297 nm, given measurements with noise but without systematic error. Integral accuracies are significantly better. The method provides a systematic way to test individual filter calibrations by examining retrievals that omit individual filters.

The resulting synthetic spectra permit the irradiance integral to be calculated for arbitrary biological action spectra, or other uses where the filter passbands by themselves do not directly constitute the needed spectral data. Further, the total ozone column and aerosol optical depths are extracted from direct irradiance measurements, if available.

Acknowledgments. This work was supported by the United States Department of Agriculture via a grant USDA CSREES # 96-34263-3527 to Colorado State University and subcontract G-1421-1, and by the Environmental Sciences Division of U.S.Department of Energy through grant number DE-FG02-90ER61072 as part of the Atmospheric Radiation Measurement Program.

References

Anderson, G. P., S. A. Clough, F. X. Kneizys, J. H. Chetwynd, and E. P. Shettle, *AGDL atmospheric constituent profiles, AFGL Tech. Rep., AFGL-TR-86-0110*, Air Force Geophys. Lab., Hanscom, AFB, Mass., 1986.

Bass, A. M., and R. J. Paur, UV absorption cross sections for ozone: The temperature dependence, *J. Photochem. 17*, 141, 1981.

Berk, A., L. S. Bernstein, and D. C. Robertson, *MODTRAN: A moderate resolution model for LOWTRAN7, AFGL Tech. Rep., AFGL-TR-89-0122*, Air Force Geophys. Lab., Hanscom, AFB, Mass., 1989.

Bigelow, D.S. , J.R. Slusser, A.F. Beaubien, and J.H. Gibson, The USDA Ultraviolet Radiation Monitoring Program, *Bull. Am. Meteorol. Soc., 79*, 601, 1998.

Booth, C. R., Synthetic UV spectroradiometry, in *IRS'96: Current Problems in Atmospheric Radiation,* edited by W. L. Smith and K. Stamnes, A. Deepak, 849pp., Hampton, Va., 1997.

Chahine, M. T., Generalization of the relaxation method for the inverse solution of non-linear transfer equations, in *Inversion Methods in Atmospheric Remote Sounding*, edited by A. Deepak, A. Deepak, 67pp, Hampton, Va., 1977.

Correll D. L., C. O. Clark, B. Goldberg, V. R. Goodrich, D. R. Hays Jr., W. H. Klein, and W. D. Schecher, Spectral ultraviolet-B radiation fluxes at the Earth's surface long-term variations at 39° N, 77° W, *J. Geophys. Res., 97* , 7579, 1992.

Dahlback, A., Measurements of biologically effective UV doses, total ozone abundances, and cloud effects with multichannel, moderate bandwidth filter instruments, *Appl. Opt., 35*, 6514, 1996.

Harrison, L. C., J. J. Michalsky, and J. Berndt, Automated multi-filter rotating shadowband radiometer: An instrument for optical depth and radiation measurements, *Appl. Opt., 33*, 5188, 1994.

Michalsky, J. J., and E. W. Kleckner, Estimation of continuous solar spectral distributions from discrete filter measurements, *Sol. Energy, 33*, 57, 1984.

Press, W. H, B. P Flannery, S. A. Teukosky, and W. T. Vetterling, *Numerical Recipes*, Cambridge Univ. Press, New York, 1989.

Stamnes, K, S.-C. Tsay, W. Wiscombe, and K. Jayaweera, Numerically stable algorithm for discrete-ordinate-method radiative transfer in multiple scattering and emitting media, *Appl. Opt., 27*, 2502, 1988.

Stephens, G. L., *Remote Sensing of the Lower Atmosphere: An Introduction*, Oxford Univ. Press, New York, 1994.

United Nations Environment Programme (UNEP), *Environmental Effects of Ozone Depletion: 1991 Update*, 1991.

VanHoosier M.E., J.-D.F. Bartoe, G.E. Brueckner, D. K. Prinz, Absolute Solar Spectral Irradiance 120nm-400nm (results from Spacelab 2), *Astrophys. Lett. and Commun., 27*, 163, 1988.

World Meteorological Organization (WMO), *Scientific Assessment of Ozone Depletion: 1994, WMO, Rep., 37,* Geneva, 1994.

Q. Min and L. Harrison, Atmospheric Sciences Research Center, State University of New York at Albany, 251 Fuller Road, Albany, New York 12203. (e-mail: min@asrc.cestm.albany.edu; lee@asrc.cestm.albany.edu)

(Received December 11, 1997; revised April 21, 1998; accepted April 24, 1998.)